Macromolecules

ARTICLE

pubs.acs.org/Macromolecules

Effect of Tear Rotation on Ultimate Strength in Reinforced Natural Rubber

Brice Gabrielle,[†,∥] Laurent Guy,[‡] Pierre-Antoine Albouy,[⊥] Loïc Vanel,[†,§] Didier R. Long,[†] and Paul Sotta*[,†]

[†]Laboratoire Polymères et Matériaux Avancés (LPMA), CNRS and Rhodia, UMR 5268, CRTL, 69192 Saint-Fons, France

[‡]Rhodia Opérations, 69660 Collonges au Mont d'Or, France

[§]Laboratoire de Physique de la Matière Condensée et Nanostructures (LPMCN), Université de Lyon, Université Lyon 1 and CNRS, UMR 5586, 69622 Villeurbanne, France

[⊥]Laboratoire de Physique des Solides, Université Paris-Sud and CNRS, UMR 5302, 91405 Orsay, France

ABSTRACT:

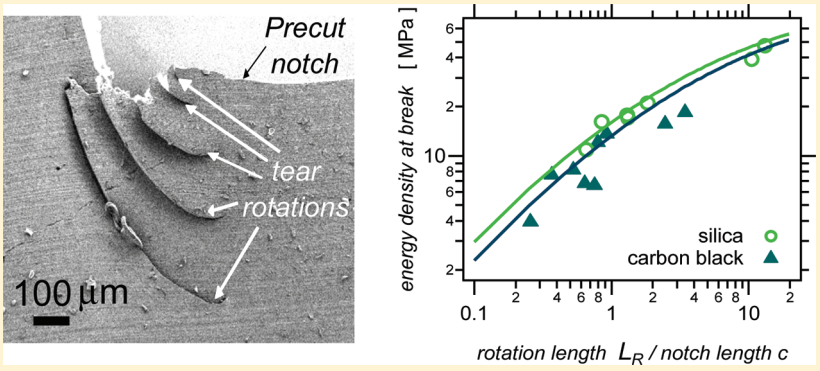

We analyze the impact of tear rotation on the tensile strength of reinforced natural rubber elastomers. Vulcanized natural rubber materials reinforced with carbon black or precipitated silica are studied. Single edge notched reinforced samples stretched at constant velocity exhibit an abrupt instability in the direction of propagation of the crack. This phenomenon has been known as tear rotation. The measured apparent tensile strength (in terms of energy at break) may be increased by a factor of 6−8 in some cases. A mechanism is proposed in order to relate the tensile strength of the material to the presence of tear rotations observed in reinforced natural rubber. This large increase in tensile strength associated with the presence of tear rotations is analyzed semiquantitatively, based on energetic arguments, without entering into a detailed description of the elastic strain field in the vicinity of the tear tip. We also show a correlation between the length of a rotation and the stress level at which it appears. The proposed interpretation is based on the idea that tear rotations relax the local strain (or stress) at the tear tip by creating a macroscopic tip radius. Materials reinforced with carbon black or precipitated silica aggregates show similar behavior.

1. INTRODUCTION

Various instabilities are observed as a crack propagates in a reinforced rubber. In trouser tests as well as in pure shear tests, so-called "knotty tearing" is observed.[1−3] In single-edge-notched tension samples (SENT) submitted to tensile loading at constant velocity, cracks tend to rotate in a direction perpendicular to the usual one, i.e., parallel to the applied tensile stress.[4] In this case, it has been called "hammer head" cracking[5] or "tear rotation". Instabilities in the direction of propagation have been quite extensively documented in carbon black (CB) filled natural rubber (NR)[4,6,7] as well as, in some cases, in CB-filled styrene−butadiene rubbers (SBR).[7]

Tensile specimens with razor cut notches of different lengths have been used to characterize resistance to tear propagation of various rubber and reinforced rubber materials.[4,8−11] It was observed that precut, filled NR samples show a much higher resistance to cut growth as compared to SBR samples and that this is associated with instabilities of the direction of tear propagation.[4,12−16] The effect of various material parameters, such as the cross-link density[9,16] and the volume fraction[17] and reinforcing power of fillers, was studied. It was already suggested that strain-induced crystallization may prevent mode I (i.e., perpendicular to the load direction) growth of the original cut notch in NR samples.[18,19] It was observed that the relation between tensile strength (or stress at break) and precut notch length is not simple in the presence of tear rotation. Various regimes of variation seem to occur in various ranges of cut length. A threshold value $c_{cr} \approx 2$ mm, above which the tensile strength drops quite abruptly, seems to be observed.[9,17] This was interpreted as corresponding to the onset of strain-induced

Received: May 12, 2011
Revised: July 5, 2011
Published: August 03, 2011

crystallization in the bulk of the test sample. This assumption will be discussed later in this paper. In some cases, it was observed that the tensile strength of carbon-black reinforced materials is reduced as compared to the pure gum.[17]

Description of crack propagation in rubbery materials is faced with two main difficulties: rubber materials can sustain extremely large elastic deformations (up to several 100%), and the viscoelastic contribution to tearing energy (dissipation) may be significant, or even perhaps dominant, in some regimes of interest, as it is evidenced by the large variation of the tearing energy with the tear propagation rate.[20,21] Moreover, dissipation is eventually not localized in a very small region close to the crack tip but may occur in a very large (macroscopic) region of the material.

At a macroscopic scale, the first approach which has been developed to analyze fracture toughness of a material is based on energetic balance arguments.[22] Here we briefly recall some basic arguments of this approach. The driving force for propagation is the energy release rate, i.e., the elastic energy recovered when a unit crack length is created by crack propagation at constant overall deformation of the test sample, denoted G in the following

$$G = -\frac{1}{e}\left(\frac{\partial U_{el}}{\partial c}\right)_{\lambda} \quad (1)$$

where e is the sample thickness, U_{el} is the elastic energy stored in the sample, W is the elastic energy density within the uniformly deformed part of the material (far away from the crack), and λ is the elongation ratio in this same part of the material, or more precisely, this would be the elongation ratio in an un-notched sample of the same overall elongation.

In the case of single-edge-notched tensile (SENT) samples, it was shown that the energy release rate G is, for a crack (precut notch) of length c, in the case of normal propagation, i.e., without instability in the direction of propagation:[23,5]

$$G \cong 2\pi\frac{Wc}{\sqrt{\lambda}} \quad (2)$$

A crack of length c becomes unstable when the energy release rate (eq 2) becomes equal to the tear energy Γ, which may be considered as a characteristic property of the material. If this instability threshold is identified with the failure of the test sample, then the following relationship between the elastic energy density stored in the material at failure W_b (energy at break) and the precut notch length c is obtained:

$$\frac{W_b}{\sqrt{\lambda_b}} = \frac{r}{2\pi c} \quad (3)$$

Note that, in the case of normal propagation, according to eq 2, the energy release rate increases as the crack length c increases. Thus, in the chosen experimental configuration (single-edge-notched tension strips (SENT samples) of finite width stretched at a given elongation rate), there is no regime of stable, slow crack growth. As a consequence, this experimental geometry does not allow controlling the crack growth rate and thus is not appropriate to characterize the tear energy vs crack growth rate curve.

In this paper, we show measurements of the tensile strength of SENT samples stretched at constant velocity. Only single propagation experiments, as opposed to cyclic (fatigue) experiments, are considered. Samples are described in section 2. Samples with different rubber matrices (SBR, NR), and different reinforcing systems (carbon black, silica with covalent coupling to the rubber matrix) are compared. We describe the tear rotation phenomenon observed in some of the samples and analyze its impact on the tensile strength of the samples (section 3) by relating the energy at break measured in prenotched tensile test samples to the overall crack contour length (which takes into account tear rotation).

Table 1. Sample Formulations[a]

formulation (phr)	SBR-s	SBR-c	NR-s	NR-c	SBR0	NR0
s-SBR 2525−0	100	100			100	
NR CV60			100	100		100
silica (Z 160 MP)[a]	50		50			
carbon black (N234)		45		45		
TESPT[b]	4		4			
6PPD[c]	1.9	1.9	1.9	1.9	1.9	1.9
stearic acid	4	4	4	4	4	4
$ZnCO_3$	4.6	4.6	4.6	4.6	4.6	4.6
Sulfur	1.5	1.5	1.5	1.5	1.5	1.5
CBS[d]	1.7	1.7	1.7	1.7	1.7	1.7
TBzTD[e]	0.24	0.24	0.24	0.24	0.24	0.24
curing time (min)	20	15	14	9	14	15

[a] Precipitated silica, surface 160 m^2g^{-1}. [b] Bis(triethoxysilylpropyl)tetrasulfur: provides covalent coupling between the matrix and silica particles. [c] *N*-(1,3-Dimethylbutyl)-*N*′-phenyl-*P*-phenylenediamine, used as antioxidant. [d] *N*-Cyclohexyl-2-benzothiazyl, used as primary accelerator. [e] Tetrabenzylthiuram disulfide, used as secondary accelerator.

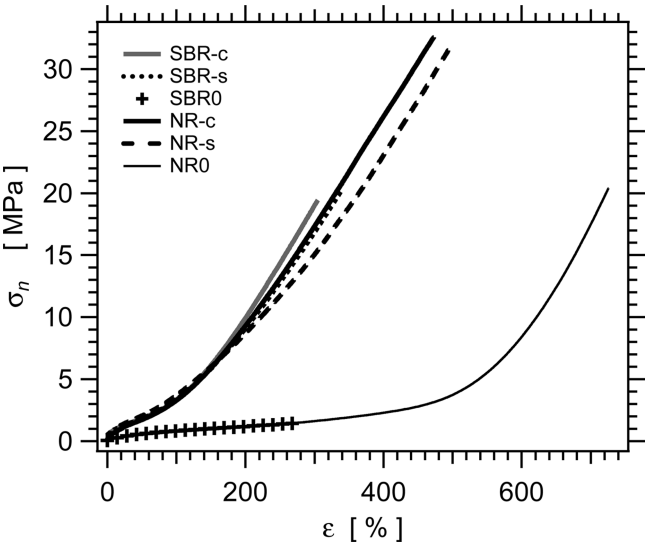

Figure 1. Nominal stress vs strain curves in the studied samples, at temperature $T = 22$ °C and strain rate 0.014 s^{-1}. End points of the curves correspond to tensile failure of the un-notched samples.

2. MATERIALS AND METHODS

In order to compare and discuss the influence of the rubber matrix and of the reinforcing filler system on tear propagation properties, six sample formulations have been used, with two types of rubber matrices (styrene butadiene rubber (SBR) and natural rubber (NR)) and two types of reinforcing fillers (carbon black and precipitated silica). Details of sample formulations are given in Table 1. In silica-filled samples, a

Table 2. Mechanical Data of the Samples, Measured in Un-Notched Tensile Strips Strained at 0.014 s^{-1}[a]

sample	nominal stress at break (MPa)	energy density at failure W_f (MPa)	modulus (MPa)
SBR0	1.85 ± 0.5	2	
NR0	17.9	14.8	
SBR-s	18.3	22	2.4
SBR-c	21.4	25.8	2.28
NR-s	29	50 ± 5	2.98
NR-c	31	55 ± 5	3.13

[a] The indicated modulus is the secant modulus (stress over strain ratio) measured in uniaxial traction (strain rate 0.014 s^{-1}) at 100% strain. This is representative of the modulus at moderate to high extension ratios (beyond the Payne effect).

coupling agent (bis(triethoxysilylpropyl)tetrasulfur, (TESPT)), which provides covalent bonding of the NR matrix to the silica surface, has to be used to obtain good reinforcement properties. Note that all samples have the same content in vulcanization ingredients, and therefore nearly the same cross-link densities. The chosen silica grade was chosen in such a way that both reinforcing systems (carbon black or silica plus coupling agent) provide the same hardness (60 Shore A) and similar reinforcement properties at the same volume fraction (about 20 vol %) in both rubber matrices, as illustrated in Figure 1. However, this may not be a general result at all filler fractions.

All experiments were carried out on a MTS 1/Me tensile apparatus with self-tightening grips and a long-range mechanical extensometer using rectangular strip pieces ($12 \times 70 \times 2$ mm^3). Single edge notched samples were precut to a length varying between roughly 0.3 and 4 mm, using a fresh razor blade dipped into a soap solution. A mechanical frame was used to ensure that the blade is perpendicular to the sample edge and the cut length constant throughout sample thickness. Cut lengths were measured afterward with a traveling microscope. Samples were stretched at a controlled, constant velocity, varying between 5 mm/min (tensile strain rate 1.4×10^{-3} s^{-1}) and 500 mm/min (tensile strain rate 0.14 s^{-1}). In tensile stress measurements, it is always somehow difficult to determine the zero stress point with high precision. Thus, a prestress with a very small value of 0.05 MPa was used to define the reference state. Experiments shown here were performed with as prepared samples, without precycling. The input energy density W is obtained by integrating the force−extension curve and dividing by the volume of the stretched sample. Note that, in precut samples, this gives only an approximation of the actual energy density stored in the material far from the tear, since in that case the strain is not uniform throughout the sample. We have chosen to use as a parameter suitable to describe tensile strength of samples the input energy density at the ultimate breaking point W_b measured for SENT samples precut at various cut lengths. Using notched samples ensures that failure will occur at a given predetermined location (the tip of the precut notch). Thus, each sample can be characterized by a characteristic relationship between the precut notch length c and the energy density at break $W_b(c)$. In a strain cycle, the energy returned on release is much smaller than the energy input on stretching (Mullins effect), even at vanishingly small strain rates. A striking relationship has been shown between the energy at break and the dissipated energy.[24,25] The dissipated energy is not available for crack propagation. The input energy may be used to characterize the sample strength in a comparative way, in order to discuss the influence of cut length and of tear rotation on it. It would not be appropriate, however, to use it in order to discuss some absolute value of the strength or of the tearing energy.

Video monitoring of crack propagation was done with an IMPERX 16M3 camera. The camera was moved at half the crosshead speed in order for the crack to remain in the image field during the tensile test. Image and data acquisitions were synchronized. Note that white dots were drawn on the surface of the samples (as seen in Figure 4). However, they were not used here to measure the strain field quantitatively, but rather to check that no slippage occurs in sample fixture grips.

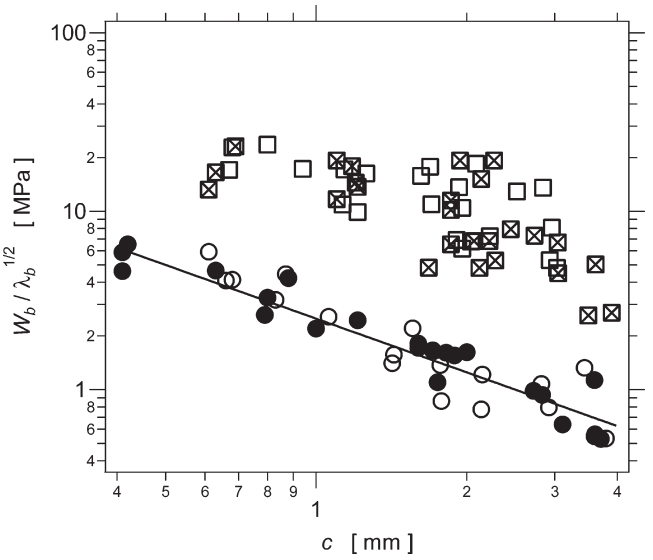

Figure 2. Quantity $W_b/(\lambda_b)^{1/2}$, where W_b is the energy density at break and λ_b the elongation ratio at break, as a function of the precut length c for various samples: NR-s (□); NR-c (box with an x); SBR-s (○); SBR-c (●). Temperature T = 22 °C.

Scanning electron microscope (SEM) observations were performed with a Zeiss SEM. The surface of the samples was metalized with platinum. Rotation lengths are measured by image analysis of SEM observations with a MatLab routine.

3. RESULTS

3.1. Estimating the Tearing Energy. We first need to characterize the behavior of unnotched samples (c = 0) in a tensile test performed at drawing speed 50 mm/min (deformation rate $\dot{\varepsilon} = 1.4 \times 10^{-2}$ s^{-1}). The corresponding nominal stress vs strain curves in the studied samples (unnotched strip samples) are shown in Figure 1. End points of the curves correspond to failure of the samples. These curves show that the reinforcement provided by either carbon black or silica, at the same volume fractions, are comparable in the studied formulations, even though stress−strain curves show significant differences in their shapes at large strain. Pure NR breaks at much larger strain and stress than SBR. It is well-known that enhanced ultimate properties of pure NR, as compared to pure SBR, are due to strain induced crystallization, which occurs around 400% strain. In filled SBR samples, both the stress and strain at break are increased compared to pure SBR. In filled NR samples, only the stress at break increases while the strain at break decreases upon addition of fillers. Nevertheless, the ultimate stress and strain of filled NR samples remain both significantly higher than for filled SBR samples. From the stress−strain curves in Figure 1, the energy density at failure W_f can be measured on uncut samples ($W_f = W_b(c = 0)$). This quantity characterizes the samples at a macroscopic scale. Its value (column 4 in Table2)

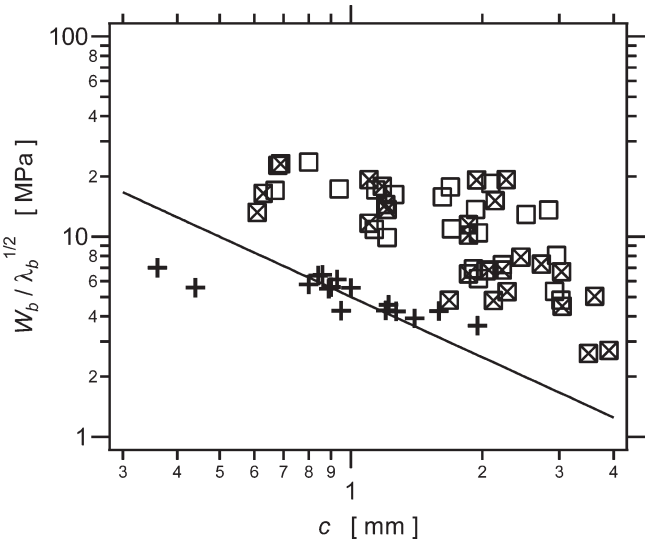

Figure 3. Quantity $W_b/(\lambda_b)^{1/2}$, where W_b is the energy density at break and λ_b the elongation ratio at break, as a function of the precut length c for samples: NR-s (□); NR-c (box with an x); NR0 (pure NR) (+). Data for reinforced NR samples (NR-s and NR-c) are the same as in Figure 2.

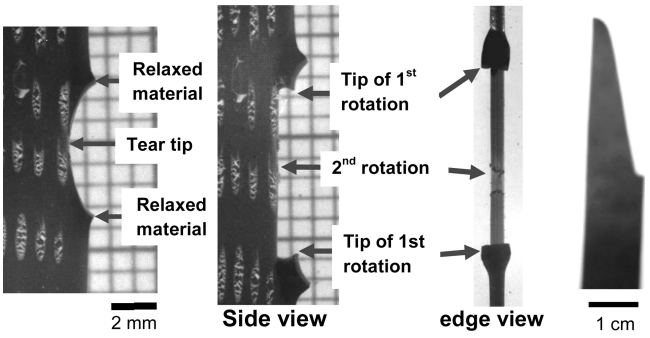

Figure 4. Macroscopic observation of successive tear rotations in a precut notched reinforced NR tensile strip. On the right is shown one part of the sample after failure. Final, catastrophic propagation deviates strongly from normal direction. White dots drawn on the sample surface appear on left two pictures. They give a qualitative impression of the strain field in the vicinity of the tear tip.

is distinct from the energy at break measured in notched test samples.

Next, we have measured the elastic energy density at break W_b of single edge notched tensile test (SENT) samples as a function of the precut notch length c, at room temperature. It is observed that slow forward propagation of the crack, if any, occurs on a very small length scale, just before fast, catastrophic failure. This slow propagation step therefore contributes only negligibly to the overall energy at break. In Figure 2, the quantity $W_b/(\lambda_b)^{1/2}$ is plotted as a function of c, according to eq 3. The results obtained in reinforced NR samples are compared to those obtained in reinforced SBR samples. Data for SBR may be reasonably fitted according to eq 3, which gives a tear energy $\Gamma_{SBR} = 15.7\ kJ \cdot m^{-2}$. Reinforced NR samples have a resistance to tear propagation (as expressed by the energy density at break W_b) typically 3 to 15 times higher than reinforced SBR. Also remarkable is the very large scattering of the reinforced NR data compared to SBR data.

The same is observed when data for reinforced NR samples are compared to pure (unfilled) NR samples (Figure 3). In this case, energy densities at break in reinforced NR are 1.5 to 8 times larger than in pure NR samples. Again, the data for pure NR are compatible with eq 3 (though in a rather limited range of precut notch length c, typically larger than 0.6 mm), which gives a tearing energy $\Gamma_{NR} = 31.4\ kJ \cdot m^{-2}$ (see Figure 3).

On the basis of the results in Figures 2 and 3, it cannot be concluded that the increased tensile strength (or average resistance to tear propagation) observed in reinforced NR as compared to pure NR and reinforced SBR may be attributed to an intrinsically higher tear energy Γ. Indeed, eq 3 does not take tear rotation into account, which provides a new mechanism of tear propagation not observed in reinforced SBR and in pure NR. Also, fitting the data for reinforced NR in Figure 2 or Figure 3 with eq 3 using a higher Γ value would not account for the large scattering of the data. Actually, when only small rotations are developed in some filled samples, the energy at break is very close to that in pure NR (see Figure 3), which indicates that the observed increase in tensile strength should rather be attributed to tear rotations than to an intrinsically higher tear energy. Despite the scattering of the reinforced NR data, Figure 3 suggests that NR have an intrinsically higher tearing energy Γ than SBR samples. This has been known already and is generally attributed to strain induced crystallization. The effect of tear rotation is quantitatively discussed in the next section.

From Figures 2 and 3, it is very difficult to discriminate the samples according to the nature of the reinforcing system. Both give widely overlapping clouds of representative points. In other words, samples formulated with a quite standard silica/coupling agent system (empty squares) have a performance comparable to those reinforced with carbon black (cross-filled square symbols) .

3.2. Tear Rotation. The tear (initiated at the precut notch) propagates in different ways in the various samples. In pure NR as well as in both pure and reinforced SBR samples, tear propagation is perpendicular to the drawing direction, as expected. Propagation occurs in a fast, catastrophic way, with relatively smooth fracture surfaces. In reinforced NR samples, tear propagation is more complex, with a well-developed tear rotation phenomenon. Both CB- and silica-filled NR samples qualitatively show the same behavior, in which three steps may be distinguished (Figure 4). First, the precut notch opens without significant propagation, up to a point at which the tear tip is widely open down to the micrometer scale. The second step is the occurrence of rotations. A tear initiates in the central region of the widely open tip, propagates perpendicularly to the tensile direction, over a small distance (typically a few tens to a few hundreds of micrometers), and then rotates abruptly on both sides along the direction of the applied force. This leads to the appearance of two rolls or folds of relaxed material curling along the crack lips in the tensile direction. Propagation along the tensile direction is slow and stops at some point. Then, as the applied load increases, a second tear eventually initiates somewhere along the straight crack tip and eventually rotates again. The whole process is illustrated in Figure 4. The successive rotations have increasing lengths and as a result, the two relaxed parts of the sample move apart from each other along the sample edge. Up to five rotations on each side may be observed successively. The propagation velocity of the rotated tear is quite slow, of the order of a few millimeters per second. The third step is the fast, catastrophic propagation starting from the last rotation, which leads to sample failure at a

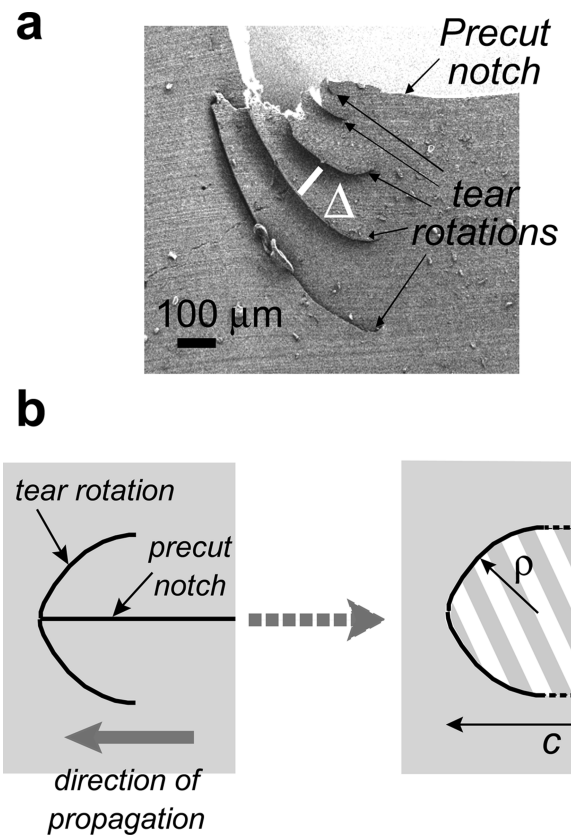

Figure 5. (a) Post mortem MEB observation of rotations in a silica filled NR sample. (b) Scheme illustrating tip blunting at a tear rotation, which effectively results in a notch of finite radius ρ. The stretching direction is vertical. The curvilinear length l_R of the rotation (measured in the relaxed state) is $l_R \cong \pi\rho$.

propagation rate of several tens of meters per second. The final, catastrophic failure itself shows large deviations of the tear propagation direction (Figure 4, right), not observed in pure NR or in reinforced SBR. Such behavior was already described in filled natural rubber materials.[4]

Here we do not analyze in detail the stress (or strain) field near the crack tip but instead propose a simple approach essentially based on energetic arguments. Specifically, we shall discuss and analyze quantitatively the effect of tear rotations on the ultimate strength of the samples.

Tear rotation enhances the tensile strength of the material, as suggested by Figures 2 and 3. Indeed, qualitatively, there seems to be a correlation between the measured energy at break and the overall length of the tear rotations: the longer the rotations, the higher the energy at break. Thus, developing long (or numerous) tear rotations allows a given sample to store more energy before it breaks, and the scattering of results obtained in reinforced NR samples (Figures 2 and 3) is related to various values of the overall tear rotation length observed for a given value of c. Successive tear rotations occur as the sample is submitted to larger and larger stretch ratios (or to larger and larger stress levels).

We propose the following analysis for the relationship between tear rotation and ultimate strength of reinforced natural rubber. After a rotation has occurred, the tear tip becomes apparently flat in the deformed state. However, when back in the relaxed state (after failure of the sample), rotations take the

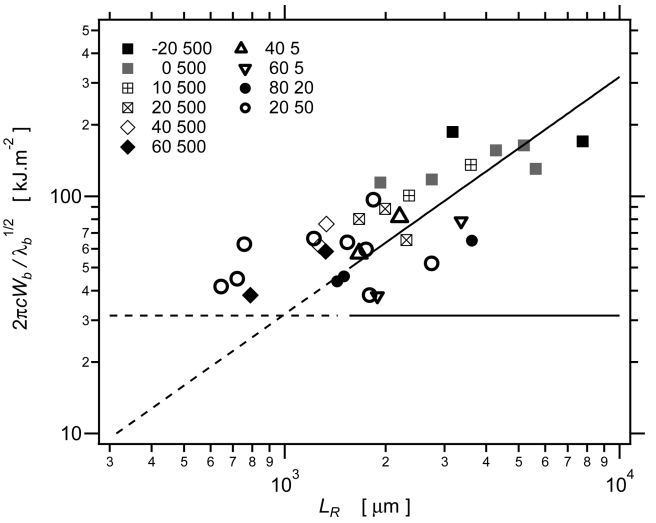

Figure 6. Quantity $2\pi cW_b/(\lambda_b)^{1/2}$ as a function of the rotation length L_R in carbon black-filled samples, for various values of the traction speed, temperature and precut notch length. Values of the temperature in °C (first number figure) and of the traction speed in mm/min (second number figure, strain rate in s^{-1} obtained by dividing by 3600) are indicated in the legend. The horizontal line indicates the value 31.4 kJ·m^{-2} obtained from the data in pure NR samples (see Figure 3). The linear curve corresponds to eq 5.

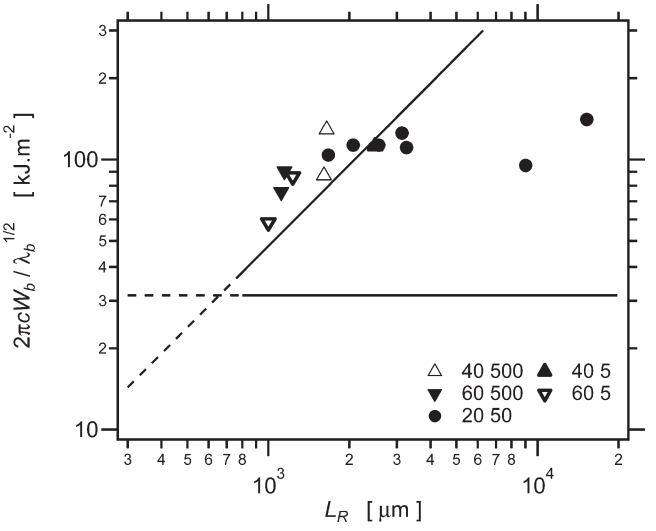

Figure 7. The quantity $2\pi cW_b/(\lambda_b)^{1/2}$ as a function of the total rotation length L_R in silica-filled samples, for various values of the traction speed, temperature and precut notch length. Values of the temperature in °C (first number figure) and of the traction speed in mm/min (second number figure, strain rate in s^{-1} obtained by dividing by 3600) are indicated in the legend. The horizontal line indicates the value 31.4 kJ·m^{-2} obtained from the data in pure NR samples (see Figure 3). The linear curve corresponds to eq 5.

form of paraboloid curves with the convexity directed toward the direction of the tear tip (see Figure 5). The part of the sample located inside the concavity of the rotation is relaxed. This situation is similar to having a cut with a finite, macroscopic radius ρ in the relaxed state (not to be confused with the opening radius at an infinitely sharp tip), as described by Thomas[26] and as studied also by Glucklich and Landel.[3]

dx.doi.org/10.1021/ma2010926 |*Macromolecules* 2011, 44, 7006–7015

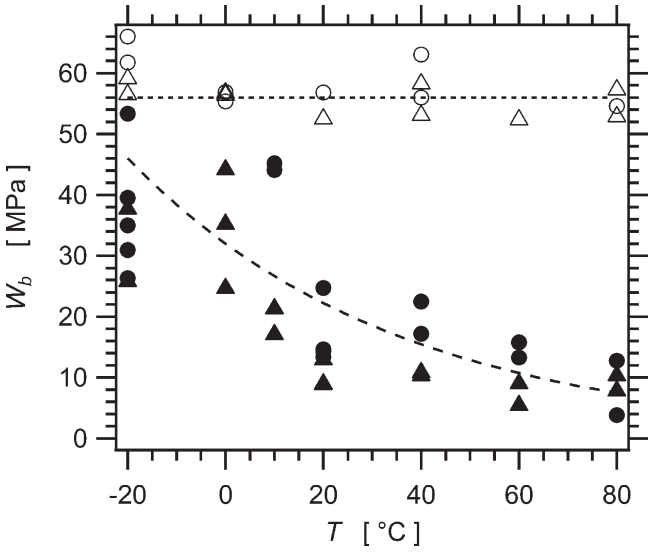

Figure 8. Energy density at break W_b as a function of temperature. Triangles: carbon black-filled samples; circles/disks: silica-filled samples. Open symbols: non precut samples; filled symbols: samples with a precut notch length $c = 2$ mm. Dashed/dotted curves are only guides to the eye.

Assuming a quasi- circular shape of the tear rotation in the relaxed state, the radius ρ is related to the measured rotation length l_R by $l_R \cong \pi\rho$ (see Figure 5). Thomas has shown the following approximate relationship between the energy release rate G and the radius ρ[26] (for a macroscopic radius ρ)

$$G \approx W_{loc}\rho \tag{4}$$

where W_{loc} is the elastic energy density at the tear tip, which is amplified with respect to the energy density far from the tip due to stress concentration. The smaller is the tip radius, the higher the stress amplification. Thus, taking $W_{loc} \cong W_f$, where W_f is the energy density at failure of the material, as the criterium for failure at the tip, eq 4 effectively corresponds to an increase of the measured value of the elastic energy density at break W_b as ρ increases. Then, identifying the energy release rate (or tearing energy) G in eq 4 to the same quantity defined in eq 2 gives the following relationship:

$$2\pi\frac{W_b c}{\sqrt{\lambda_b}} = W_f\frac{l_R}{\pi} \tag{5}$$

This equation relates the ultimate property of a sample, through the quantity $2\pi cW_b/(\lambda_b)^{1/2}$ (which is homogeneous to a tearing energy, expressed in kJ·m^{-2}), to the length of the last rotation l_R. The quantity $2\pi cW_b/(\lambda_b)^{1/2}$ is plotted in Figure 6 and Figure 7 as a function of the total rotation length L_R for experiments done on notch tensile strips with various precut notch length values, stretched at different traction speeds and temperatures, in samples reinforced with carbon black and silica, respectively. Note that L_R is the total rotation length of all rotations. It is however largely dominated by the length of the ultimate rotation. The horizontal line in Figures 6 and 7 corresponds to the value of the tearing energy 31.4 kJ·m^{-2}. The linear curves in both figures correspond to eq 5. The slopes (denoted W_f/π in eq 5) have been tuned to match the data qualitatively. The corresponding values correspond to $W_f = 100$ MPa and $W_f = 150$ MPa for carbon black- and silica-filled samples, respectively. These values are only semiquantitative, and we shall not discuss them in terms of differences between both types of samples. Nevertheless, it is important to notice that these values are larger than the energy at break measured in the uncut samples (see Table 2). This is to be expected because both quantities are different in nature. The strength W_f is larger than W_b (macroscopically measured on uncut test samples) because it is a local quantity. The macroscopically measured tensile energy W_b depends on the typical size and nature of the flaws (or local stress heterogeneities) which are present within the material.

Thus, Figures 6 and 7 show that eq 5 is semiquantitatively verified, or at least gives the right order of magnitude for the relationship between the ultimate property (as expressed by the quantity $2\pi cW_b/(\lambda_b)^{1/2}$) and the rotation length. The large apparent scattering of points is mainly related to the fact that points obtained in different experimental conditions are plotted together. This allows one to see that temperature seems to have an effect on tear rotations. Tear rotations tend to be longer on average at low temperature. In carbon black-filled samples, rotation lengths L_R measured in samples stretched at −20, 0, and +10 °C are between 2 and 9 mm, whereas those measured at higher temperatures (40 °C and above) are between 0.6 and 3 mm typically. In silica-filled samples, rotation lengths measured at 40 °C and above are between 2 and 10 mm; those at 20 °C are on the order of 1 mm. On the other hand, varying the traction speed does not have a significant effect in the investigated strain rate range between 1.4×10^{-3} s^{-1} and 0.14 s^{-1}.

The energy density at break in un-notched samples does not depend significantly on temperature, in the range −20 to 80 °C. On the other hand, the energy at break measured in precut samples does depend on temperature, as illustrated in Figure 8. From the previous discussion, this effect may be entirely due to the variation of the average tear rotation length as a function of temperature. Note also that, at comparable energy at break, the overall rotation length tends to be larger in samples stretched at low traction speeds.

It is clear from Figures 6 and 7 that the data show a tendency to deviate from the linear variation expressed in eq 5. This deviation may be interpreted semiquantitatively in the following way. For a tear of length c and finite tip radius ρ (in the relaxed state), from standard elasticity in the linear regime, the elastic stress remains finite at the tip and is given by

$$\sigma_t \approx \left(1 + 2\left(\frac{c}{\rho}\right)^{1/2}\right)\sigma_0 \tag{6}$$

where σ_0 is the stress in the homogeneously stretched part of the sample, far away from the tear tip. In terms of energy density (taking an energy density quadratic in the stress), this writes:

$$W_{loc} \approx \left(1 + 2\left(\frac{c}{\rho}\right)^{1/2}\right)^2 W_0 \tag{7}$$

W_0 is the elastic energy density far from the tip. Note that in general ρ is not small compared to c here. In the same way as for eq 5, we assume that initiation of propagation (which corresponds to the detected onset of the next rotation) will occur when the local energy density W_{loc} reaches some characteristic input energy density at failure of the material

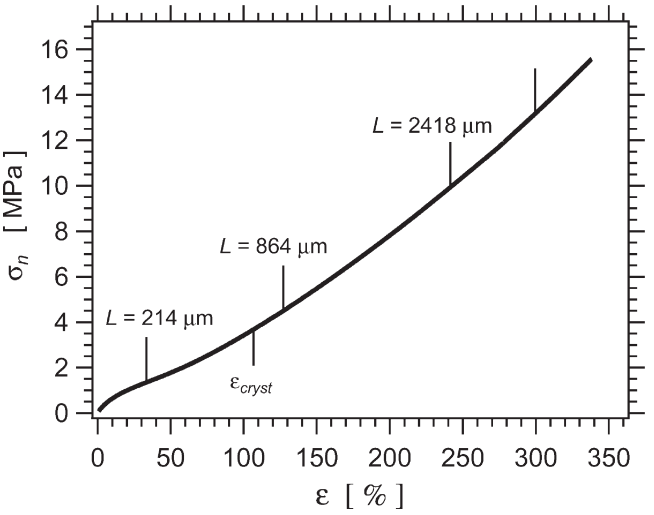

Figure 9. Nominal stress σ_n as a function of the macroscopic deformation in a precut silica-filled NR sample stretched up to failure (precut notch length c = 2 mm). The onsets of successive tear rotations are indicated, together with the length of the corresponding rotation. The last rotation initiates around 300% overall strain, it propagates along the applied extension until it leads to failure at about 340%. The onset of strain-induced crystallization in the bulk ε_{cryst} (i.e., in a uncut, uniformely stretched sample) is also indicated.

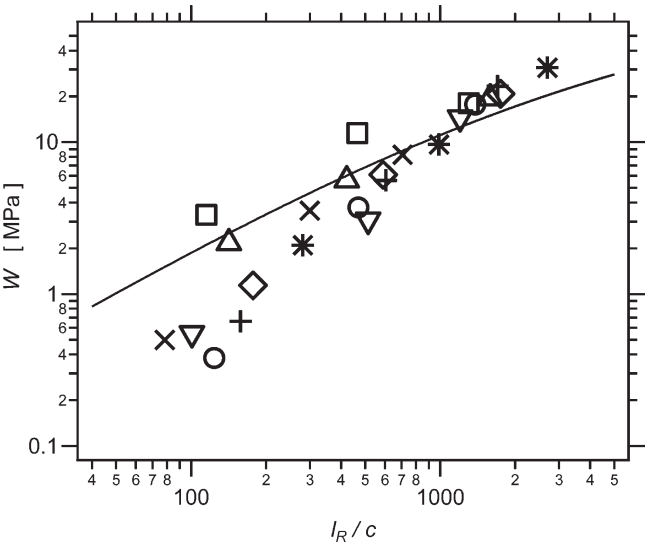

Figure 10. Elastic energy density $W(n+1)$ at the onset of tear rotation $n+1$ (for n = 0 to 2), as a function of the ratio $l_R(n)/c$ in silica-filled samples (NR-s). $l_R(n)$ is the length of rotation n in μm (which determines the effective tear tip radius), c is the precut notch length in mm. Each type of symbol corresponds to a particular test sample. For each sample, data were collected as indicated for one example in Figure 9. The curve corresponds to eq 9.

W_f. This leads to the relationship:

$$W_b \approx \left(1 + 2\left(\frac{c}{\rho}\right)^{1/2}\right)^{-2} W_f \qquad (8)$$

Assuming that the contour length l_R of the rotation (in the relaxed state) is proportional to its radius in the relaxed state (typically $l_R \approx \pi\rho$), in the same way as before, leads to

$$W_b \approx \left(1 + \kappa\left(\frac{c}{l_R}\right)^{1/2}\right)^{2} W_f \qquad (9)$$

in which κ is a geometrical, dimensionless parameter of order $2\sqrt{\pi}$.

Actually, eq 9 (as well as eq 5) gives a relationship between the radius of the crack (related to the length l_R of a given rotation, say rotation number n) and the onset of crack instability $W_b(n+1)$, assumed to correspond to initiation of the next tear rotation (rotation number $n+1$) or to the onset of propagation leading to final break of the sample.

An example of stress−strain curve obtained in a precut sample up to failure, in which the onsets of successive tear rotations have been determined by video monitoring, is shown in Figure 9. The onsets of successive tear rotations are indicated on the curve, together with the length (in μm) of the corresponding rotation. Note that no large scale artifact occurs on the stress strain curve when a rotation appears and propagates.

Data illustrating eq 9 are shown in Figure 10 for a series of samples with various precut notch lengths c (between 0.95 and 3.5 mm) exhibiting tear rotations (typically three rotations are observed before final rupture). The threshold at initiation of a given rotation (corresponding to the quantity $W_b(n)$ in eq 9) is plotted as a function of the length of the previous rotation ($l_R(n-1)$ in eq 9). Note that the first rotation, which is very short and difficult to measure (see Figure 5a), is not taken into account in Figure 10. The curve corresponds to eq 9. The values of the parameters which have been used here are W_f = 100 MPa and κ = 2.0.

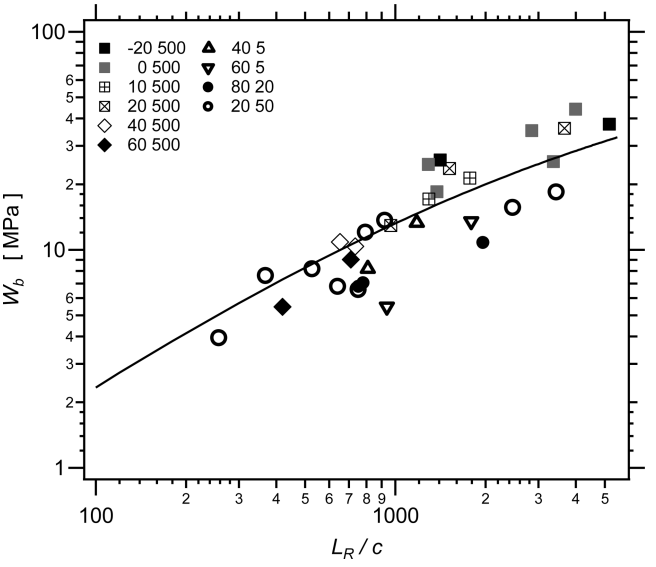

Figure 11. Energy density at break W_b as a function of the reduced total rotation length L_R/c (L_R is in μm, c in mm) in carbon black-filled NR samples, stretched at various traction speeds and temperatures (from the same set of experimental data as in Figure 6). The curve corresponds to eq 9.

The correlation between the energy at break and the rotation length is also illustrated in Figure 11 and Figure 12, which show the elastic energy density at break W_b as a function of the reduced total rotation length L_R/c, in samples reinforced with carbon black and silica, respectively. Results obtained at

dx.doi.org/10.1021/ma2010926 |Macromolecules 2011, 44, 7006–7015

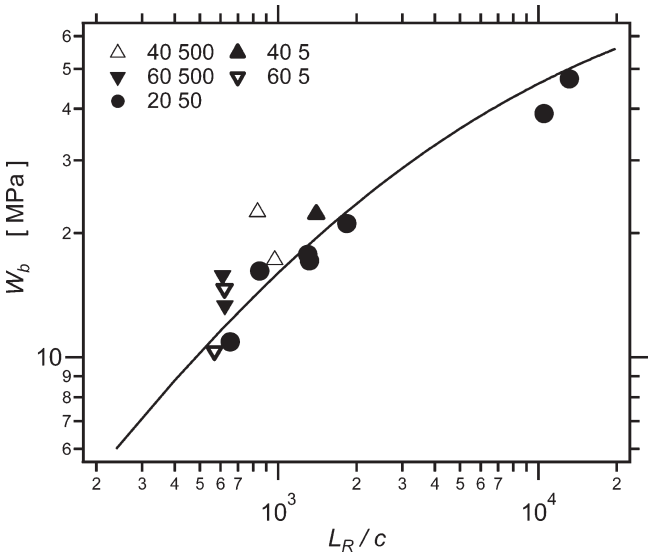

Figure 12. Energy density at break W_b as a function of the reduced total rotation length L_R/c (L_R is in μm, c in mm) in silica-filled NR samples, stretched at various traction speeds and temperatures (from the same set of experimental data as in Figure 7). The curve corresponds to eq 9.

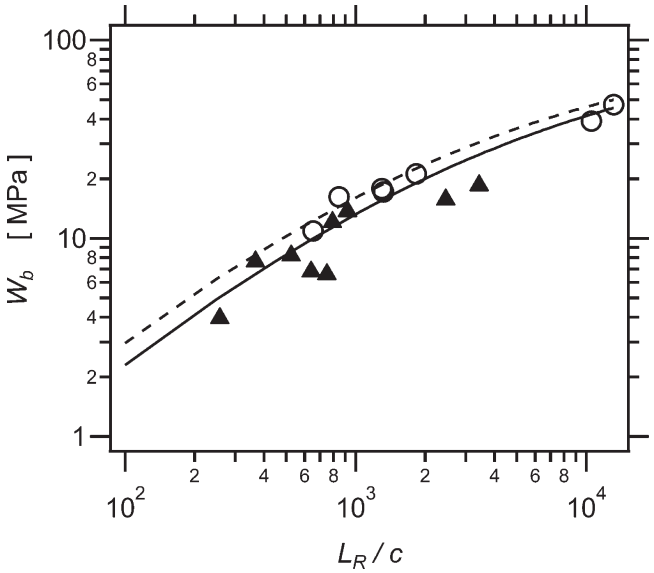

Figure 13. Energy density at break as a function of the reduced total rotation length L_R/c (L_R is in μm, c in mm) in carbon black-filled (full triangles) and silica-filled (circles) samples, measured at strain rate 1.4×10^{-2} s^{-1} and T = 22 °C. Curves are fits to eq 9, using the same sets of parameters as in Figure 11 and Figure 12: W_f = 100 MPa, κ = 1.5 (silica-filled samples, dashed curve); W_f = 100 MPa, κ = 1.75 (carbon black-filled samples, full curve).

different values of the traction speed and temperature, corresponding to the same data as in Figures 6 and 7, are shown. The curves in Figures 11 and 12 correspond to eq 9. The following sets of parameters have been used to match the data: silica-filled samples, W_f = 100 MPa, κ = 1.5; carbon black-filled samples, W_f = 100 MPa, κ = 1.75.

Finally, data obtained at room temperature and a tensile rate of 0.014 s^{-1} are shown in Figure 13 for samples reinforced with carbon black and silica. Both sets of data have been matched with eq 9, using for each type of sample the same set of parameters as in Figures 11 and 12, that is: silica-filled samples, W_f = 100 MPa, κ = 1.5; carbon black-filled samples, W_f = 100 MPa, κ = 1.75. Silica-filled samples tend to show slightly longer rotations than CB-filled samples.

4. DISCUSSION

The results shown here are coherent with previously published results.[11] In particular, reinforced SBR samples studied in ref 11 do not show longitudinal propagation (i.e., tear rotation). However, in other publications, it is observed that reinforced SBR samples exhibit instabilities of the direction of crack propagation as well,[10] in the form of so-called "knotty tearing". However, it does not seem that knotty tearing in reinforced SBR samples lead to rotations as described here and illustrated in Figure 5a. Abrupt bifurcation of propagation direction in the longitudinal direction (along the traction direction) with subsequent arrest of propagation, is a mechanism distinct from knotty tearing as described in SBR (and perhaps in other types of noncrystallizing reinforced elastomers as well), which comes from local heterogeneities of the stress field, not necessarily associated with local anisotropy of the material constitutive law.

For the first time, a mechanism is proposed to analyze the measured tensile strength of a reinforced natural rubber material in the presence of tear rotations. The mechanism which we propose to describe the tear rotation pattern is the following one: when the test sample is stretched at a given extension rate, the precut notch opens widely without visible propagation, as long as the local energy density at the tear tip W_{loc} remains below a critical value W_f for initiation of propagation. When $W_{loc} = W_f$, propagation initiates. After propagating over a few 10s of μm, the tear rotates. Tear rotation effectively releases part of the stress amplification at the tear tip, by creating a *macroscopic* tear tip radius ρ (which scales as and is comparable to the rotation length). This may provide a purely elastic mechanism for effective tip blunting, distinct from the Dugdale-Barenblatt visco-plastic mechanism.[27,28] In the rotated tear configuration, the relationship between the macroscopic energy density W_0 (far away from the tear) and the local energy density at the tear tip W_{loc} is given by eq 7. Then the test sample can be further stretched, until the local energy density at the tear tip reaches again the critical value W_f. Thus, in this proposed mechanism, each successive rotation effectively results in a larger tip radius, which allows reaching larger macroscopic values of the elastic energy density in the bulk of the sample, according to eq 7.

Equations 6 and 7 and the resulting eq 9 have been written by assuming linear elasticity, which of course is not valid in rubbers at the very large local strain values considered here. However, the analysis proposed here is only semiquantitative. The data have a quite large statistical scattering whatsoever. Taking nonlinearities into account would not change the analysis and the conclusions. The proposed mechanism allows matching the data quite well with eq 9, which contains two parameters: the local energy density at onset of propagation (denoted W_f), which is coherently larger than the tensile strength of bulk (non precut) samples; a geometrical factor κ. The value of this factor would certainly be affected by non linearities, but its order of magnitude should essentially be preserved.

The tear rotation phenomenon observed here and illustrated in Figure 4 has some similarities with the transition between cohesive and interfacial failure in a laminate described by

dx.doi.org/10.1021/ma2010926 |*Macromolecules* 2011, 44, 7006–7015

Kendall.[29] Both situations are different, however. Kendall describes a situation in which a crack propagating in a material (in mode I) meets a perpendicular interface, and examines the conditions under which the crack may be deflected along this weaker interface. In the present case, a weaker interface (characterized by a given cohesive energy) does not preexist in the material. Such an interface must therefore be created within the material during crack propagation itself. This phenomenon has been attributed to the occurrence of strain-induced crystallization in NR and in filled NR.[30−34] The onset of strain induced crystallization in a bulk (non precut, homogeneously strained) sample, as detected by X-ray scattering, is indicated in Figure 9. It is interesting to note that the first rotation occurs below the crystallization threshold, that is, before the whole test sample crystallizes in bulk. Nevertheless, due to local strain amplification, the material crystallizes in the vicinity of the tear tip quite early before the whole test sample crystallizes in bulk.[19,35] Preliminary, qualitative estimate of strain amplification at the tear tip indicate that the strain may be amplified to a factor of 3 at least. The extension of the semicrystalline region depends on the overall extension ratio (far from the tear tip) and becomes infinite at the onset of bulk crystallization. It is likely that the presence of this crystallized region prevents the tear to propagate forward in the normal direction (perpendicular to the direction of extension) because it induces a strong elastic anisotropy in the material, which could be the main mechanism responsible for tear rotation.

However, strain induced crystallization by itself is not sufficient to induce tear rotation, as pure NR samples (which do crystallize) do not exhibit tear rotation. A combination of strain-induced crystallization and of reinforcement provided by nanometric fillers, which both shift the onset of crystallization to lower overall strain and considerably increase the modulus, is thus needed to induce this phenomenon. Also, it is worth mentioning that tear rotation does not appear in the absence of a precut notch (of millimeter size).

We have checked that strain induced crystallization takes place in the whole temperature range investigated (i.e., up to 80 °C), with ultimate crystallinity and critical strain at onset little affected by temperature in this range. On the other hand, it is likely that crystallization kinetics is fast enough to remain unaffected or only little affected by the traction speed, in the investigated range of values. A detailed study of strain induced crystallization in our materials will be published separately.

It is observed that the material exhibits well developed fibrilar morphology at very high extension ratios. Then it is likely that such fibrils have a very high modulus (that of a semicrystalline polymer) in the presence of strain-induced crystallization, thus providing the strong anisotropy in the elastic properties needed to observe tear rotation. Indeed, such anisotropy could favor propagation along the tensile direction, as compared to normal propagation (perpendicular to tensile direction). However, the anisotropy in local elastic properties has not been quantified (equivalent to the ratio of cohesive vs adhesive energies as discussed by Kendall) and thus the conditions for onset of tear rotation are not discussed here.

The argument developed in section 3.2 does not apply to the first rotation, which initiates in the tip of the precut notch itself (with a micrometric tip radius). The occurrence and size of the first rotation may be analyzed as follows, using qualitative arguments based on linear elasticity. For a cut of length c with an infinitely sharp tip, standard linear elasticity gives a parabolic opening of the tear tip, with an opening radius in the deformed state (not to be confused with the finite tip radius created through tear rotation, denoted ρ previously):

$$R = \frac{1}{4\pi}\left(\frac{3K}{E}\right)^2 \approx \frac{3}{4}\frac{{\sigma_0}^2 c}{E^2} \approx \frac{3}{2}\frac{Wc}{E} \tag{10}$$

Here $K = \sigma_0(\pi c)^{1/2}$ is the stress intensity factor (in opening mode I), E is the Young's modulus, and $W = {\sigma_0}^2/2E$ is the strain energy density far from the tear. The Poisson ratio has been taken to be $\nu = 0.5$, the value for an incompressible material. Now we make the assumption that the length l_R of the first rotation (in the deformed state) scales as, and is of the order of, the tip opening radius R (perhaps within a geometrical factor), which is the only characteristic length scale at the tear tip in the deformed state (neglecting finite size effects). According to eq 10, it follows that W is proportional to l_R:

$$l_R \approx \frac{Wc}{E} \tag{11}$$

The first rotation occurs at a strain energy density of the order $W \approx 0.2-0.4$ MPa with the precut notch length $c = 2$ mm (see Figure 9). The modulus is of the order 3 MPa (see Table 2). Equation 11 then gives $l_R \approx 0.2-0.5$ mm (in the deformed state). Assuming a local strain of the order 5 (typical value of the strain at break, as illustrated in Figure 1), this corresponds to a length in the relaxed state on the order of 0.04−0.1 mm, which is indeed the right order of magnitude, as seen for one example in Figure 5 a. Note that this argument relates W to l_R for the first rotation, but does not give the value of the onset of propagation for this rotation. The value of the onset for a given precut notch length c is rather given by eq 3.

Finally, tear rotations have little effect on the stress−strain curves, as is illustrated in Figure 9. This is very different from the large oscillations of the tearing force which are observed e.g. in tearing tests performed in the trouser geometry.[36] Only in some cases, with very large tear rotations, stress−strain curves exhibit some visible accidents, which are very much reminiscent of the large oscillations of the tearing force observed in the regime of so-called knotty tearing in the trouser test geometry. The drop in the force corresponds to forward tear propagation. Then, as tear deviates from its normal direction, the force start to increase again, as propagation along the direction of extension corresponds to a vanishing energy release rate.

We have compared NR samples reinforced with carbon black and precipitated silica. Both types of samples were formulated in order to have similar cross-link densities, filler volume fractions, and altogether have quite similar mechanical properties. Both types of samples show very similar behavior as regards the development of tear rotation and resulting tensile strength, in the whole temperature range investigated here.

5. CONCLUSION

For the first time, a mechanism is proposed to relate the presence of tear rotations observed in reinforced natural rubber to the tensile strength of the material. The proposed arguments may be used to predict the resistance to tear of various reinforced natural rubber materials, based on the observation and analysis of the tear rotation patterns. The measured apparent tensile strength (in terms of input energy at break) may be increased by a factor of 6−8 in some cases. This large increase in tensile strength associated with the presence of tear rotations is analyzed

semiquantitatively, based on energetic arguments, without entering into a detailed description of the elastic strain field in the vicinity of the tear tip. We show a correlation between the extent of the phenomenon of tear rotation and the input energy density at failure of single edge notched tensile test samples. We also show a correlation between the length of a rotation and the stress level at which it appears. The proposed interpretation is based on the idea that tear rotations relax the local strain (or stress) at the tear tip by creating a macroscopic tip radius. This is a mechanism of tip blunting which is different from visco-plastic effects described first by Dugdale and Barenblatt. Materials reinforced with either carbon black or silica (with TESPT as coupling agent), formulated to have close mechanical behavior, show similar behavior.

AUTHOR INFORMATION

Present Addresses

[||] Institut de Chimie et des Matériaux Paris-Est (ICMPE), CNRS/Université Paris XII - Val de Marne, UMR 7182, 2−8, rue Henri Dunant, 94320 Thiais, France

REFERENCES

(1) Greensmith, H. W. *J. Polym. Sci.* **1956**, *21*, 175–187.
(2) Greensmith, H. W. *J. Appl. Polym. Sci.* **1960**, *3*, 183–193.
(3) Glucklich, J.; Landel, R. F. *J. Appl. Polym. Sci.* **1976**, *20*, 121–137.
(4) Hamed, G. R.; Kim, H. J.; Gent, A. N. *Rubber Chem. Technol.* **1996**, *69*, 807.
(5) Lake, G. J.; Samsuri, A.; Teo, S. C.; Vaja, J. *Polymer* **1991**, *32*, 2963–2975.
(6) Busse, W. F. *Ind. Eng. Chem.* **1934**, *26*, 1194–1199.
(7) Stacey, R.; Yanyo, L.; Kelley, F. *Rubber Chem. Technol.* **1986**, *58*, 421.
(8) Thomas, A. G.; Whittle, J. M. *Rubber Chem. Technol.* **1970**, *43*, 222.
(9) Hamed, G. R.; Rattanasom, N. *Rubber Chem. Technol.* **2002**, *75*, 935–941.
(10) Goldberg, A.; Lesuer, D.; Patt, J. *Rubber Chem. Technol.* **1989**, *62*, 288–304.
(11) Hamed, G.; Park, B. H. *Rubber Chem. Technol.* **1999**, *72*, 946.
(12) Kim, H. J.; Hamed, G. *Rubber Chem. Technol.* **2000**, *73*, 743.
(13) Hamed, G.; Kim, H. J. *Rubber Chem. Technol.* **1999**, *72*, 895.
(14) Hamed, G.; Huang, M. Y. *Rubber Chem. Technol.* **1998**, *71*, 846.
(15) Hamed, G.; Zhao, J. *Rubber Chem. Technol.* **1998**, *71*, 157.
(16) Hamed, G.; Rattanasom, N. *Rubber Chem. Technol.* **2002**, *75*, 323.
(17) Hamed, G.; Al-Sheneper, A. A. *Rubber Chem. Technol.* **2003**, *76*, 436.
(18) Andrews, E. H. *J. Appl. Phys.* **1961**, *32*, 542–548.
(19) Lee, D. J.; Donovan, J. A. *Rubber Chem. Technol.* **1987**, *60*, 910–923.
(20) Persson, B. N.; Albohr, O.; Heinrich, G.; Uebas, H. *J. Phys.: Condens. Matter* **2005**, *17*, R1071–R1142.
(21) Lake, G. J.; Lawrence, C. C.; Thomas, A. G. *Rubber Chem. Technol.* **2000**, *73*, 801–817.
(22) Rivlin, R. S.; Thomas, A. G. *J. Polym. Sci.* **1953**, *10*, 291.
(23) Lake, G. J. In *Proceedings of the International Conference on Yield, Deformation and Fracture of Polymers, Cambridge*; Institute of Physics: London, 1970; p 5.3/1.
(24) Grosch, K.; Harwood, J. A.; Payne, A. R. *Nature* **1966**, *212*, 497.
(25) Harwood, J. A.; Payne, A. R. *J. Appl. Polym. Sci.* **1968**, *12*, 889–901.
(26) Thomas, A. G. *J. Polym. Sci.* **1955**, *18*, 177–188.
(27) Dugdale, S. D. *J. Mech. Phys. Solids.* **1960**, *8*, 100.
(28) Barenblatt, G. I. *Adv. Appl. Mech.* **1962**, *7*, 55.
(29) Kendall, K. *Proc. R. Soc. London A* **1975**, *344*, 286–302.
(30) Gent, A. N. *Trans. Faraday Soc.* **1954**, *50*, 521.
(31) Miyamoto, Y.; Yamao, H.; Sekimoto, K. *Macromolecules* **2003**, *36*, 6462–6471.
(32) Poompradub, S.; Tosaka, M.; Kohjiya, S.; Ikeda, Y.; Toki, S.; I., S.; Hsiao, B. S. *J. Appl. Phys.* **2005**, *97*, 103529.
(33) Chenal, J.; Gauthier, C.; Chazeau, L.; Guy, L.; Bomal, Y. *Polymer* **2007**, *48*, 6893–6901.
(34) Rault, J.; Marchal, J.; Judeinstein, P.; Albouy, P. A. *Macromolecules* **2006**, *39*, 8356–8368.
(35) Trabelsi, S.; Albouy, P.; Rault, J. *Macromolecules* **2002**, *35*, 10054–10061.
(36) Stacer, R. G.; Von Meerwall, E. D.; Kelley, F. N. *Rubber Chem. Technol.* **1986**, *58*, 913.